A lamellar model for the X-ray rocking curves of sagittally bent Laue crystals

Z. Zhong,[a]* C. C. Kao,[a] D. P. Siddons,[a] H. Zhong[b] and J. B. Hastings[a]†

[a]National Synchrotron Light Source, Brookhaven National Laboratory, Upton, NY 11973, USA, and [b]Department of Mechanical Engineering, University of Akron, Akron, OH 44325-3903, USA. Correspondence e-mail: zhong@bnl.gov

The use of sagittally bent asymmetric Laue crystals in horizontally focusing monochromators for high-energy synchrotron X-rays necessitates simulation of the X-ray reflectivity by such crystals. Based on the theory of the lattice distortion in the diffraction plane of sagittally bent Laue crystals, a lamellar model was developed to predict their rocking curves. The model was experimentally verified by rocking-curve measurements from various reflections on silicon crystals of four representative orientations, sagittally bent to various radii, using X-rays of 67 keV energy.

1. Introduction

We showed that sagittally bent asymmetric Laue crystals can focus X-rays horizontally (Zhong *et al.*, 2001*a*). The combination of a Laue crystal's small beam footprint and the use of inverse Cauchois geometry through anticlastic bending results in double-crystal sagittally focusing monochromators ideally suited for high-energy synchrotron X-rays (Zhong *et al.*, 2001*b*). The intensity of the X-rays produced by such a device utilizing identical sagittally bent Laue crystals is proportional to the integrated reflectivity of the first crystal, and the reflectivity of the second one. Thus, it is desirable to simulate the reflectivity and the integrated reflectivity of such crystals so that, with this knowledge, the design of the monochromator can be optimized for specific experimental needs.

Meridionally bent perfect crystals (crystals bent in the diffraction plane) have been used to meridionally focus X-rays and neutrons, and as non-focusing monochromators and analyzers to provide adjustable bandwidth. Various lamellar models were developed for such crystals, bent cylindrically or spherically, and diffracting in the Bragg or Laue geometry, to calculate their diffraction properties (White, 1950; Egert & Dachs, 1970; Albertini *et al.*, 1976; Boeuf *et al.*, 1978; Mikula *et al.*, 1984; Erola *et al.*, 1990; Suortti *et al.*, 1990).

Although the lamellar model is less precise than some more elaborate ones (Penning & Polder, 1961; Kalman & Weissmann, 1983; Schulze & Chapman, 1995), it provides the shape of the rocking curve, in addition to the integrated reflectivity, and relates these properties to the local strain across the depth of a distorted crystal. Thus, it has been widely used for moderately to severely distorted crystals. However, owing to the difference between crystals bent sagittally and meridionally, a lamellar model for meridionally bent Laue crystals cannot be adapted simply for sagittally bent ones (Zhong *et al.*, 2001*b*).

A model for the rocking-curve width of sagittally bent Laue crystals was recently introduced, taking into consideration the elastic anisotropy which plays an important role in X-ray diffraction by sagittally bent silicon crystals (Zhong *et al.*, 2002). The model relates the strain in the diffraction plane to the sagittal bending. The validity of the basic assumption of the lamellar model for these crystals, *i.e.* the strain-induced gradual change of the Bragg condition through the crystals, also was verified by depth-resolved rocking-curve measurements.

Here, we use this understanding as a basis for a lamellar-model calculation of the reflectivity and integrated reflectivity of sagittally bent Laue crystals. We verified the model by measuring the rocking curves of different reflections, using sagittally bent Laue crystals of different orientations.

2. Lamellar model for sagittally bent Laue crystals

Fig. 1(*a*) shows a planar Laue crystal, sagittally bent to a radius R_s. The diffraction vector **H** lies in the plane of diffraction which coincides with the plane of the paper. The crystal is approximated by a stack of perfect lamellae with a gradually changing angle (in the diffraction plane) and lattice spacing. Thus, the Bragg condition changes progressively for lamellae along the path of the incident beam.

$\Delta\theta_{\rm rot}(T)$, defined as the change in the angle of the lamellae at depth T with respect to that at $T = 0$ along the path of the incident beam, is (Zhong *et al.*, 2002)

$$\Delta\theta_{\rm rot}(T) = \mp \frac{T}{R_s}[(S'_{13} - CS'_{23})\sin\chi\cos\chi - CS'_{23}\tan(\chi \mp \theta_B) + S'_{36}\cos^2\chi], \qquad (1)$$

where θ_B is the Bragg angle, χ is the asymmetry angle for the Laue reflection (defined as the angle between the lattice planes and the crystal's surface normal), C is a measurable

constant, typically 0.2–1, that accounts for the constraints on the crystal (Krisch *et al.*, 1991; Suortti & Schulze, 1995; Yoneda *et al.*, 2001), $S'_{ij} \equiv S_{ij}/S_{33}$ and S_{ij} are the orientation-dependent elastic compliances of the crystal. χ is positive if the diffraction vector is in the first and third quadrants (as is the case in Fig. 1*a*), and otherwise negative. The upper signs are used when **H** is in the first and second quadrants, as shown by the solid **H** vector in Fig. 1(*a*); the lower signs are used when it is in the third and fourth quadrants, as shown by the dashed **H** vector. $\Delta\theta_{\mathrm{rot}}(T)$ is due to the combined effects of the geometrical curvature of the crystal in the diffraction plane [represented by the $CS'_{23}\tan(\chi \mp \theta_B)$ term] and the tilting of the lattice planes as a result of anticlastic ($CS'_{23}\sin\chi\cos\chi$ term) and sagittal curvature (S'_{13} and S'_{36} terms).

The relative change in Bragg angle, $\Delta\theta_B(T)$, of the lamellae at depth T is (Zhong *et al.*, 2002)

$$\Delta\theta_B(T) = -(T/R_s)\tan\theta_B[S'_{13}\sin^2\chi + CS'_{23}\cos^2\chi \\ + S'_{36}\sin\chi\cos\chi]. \tag{2}$$

$\Delta\theta_B(T)$ is due to stretching or compression of the lattice planes.

The angle the crystal must rotate to satisfy the Bragg condition for the lamella at depth T then is

$$\Delta\theta(T) = -\Delta\theta_{\mathrm{rot}}(T) + \Delta\theta_B(T) \tag{3}$$

$$\equiv \frac{T}{R_s}\frac{1}{\gamma_0 B(\theta_B, \chi, S')}, \tag{4}$$

where $\gamma_0 = \cos(\chi \mp \theta_B)$ and $B(\theta_B, \chi, S')$ is a unitless constant, following the notation of Erola *et al.* (1990). B depends on the crystal's orientation (through S') and reflection (through θ_B and χ), and can be calculated using (1), (2) and (3) for a given reflection and crystal orientation.

Fig. 1(*b*) illustrates the lamellar-model assumptions for X-ray diffraction by a sagittally bent Laue crystal. Both the change in the angle and the lattice spacing of the lamellae along the path of the incident beam contribute to a change in the Bragg condition, determined by (3). By properly choosing the thickness of the lamellae, this change is small enough so that a lamella may be treated as a perfect crystal using the dynamical theory of X-ray diffraction (Batterman & Cole, 1964). If the lamellar thickness, T_l, is chosen such that $\Delta\theta(T_l)$ across the lamella is close to the Darwin width of the reflection used, then the reflectivity calculated by integrating the dynamical diffraction of the lamellae agrees with experimental results (Suortti & Thomlinson, 1988). The dynamical-theory reflectivity of a lamella satisfying the Bragg condition and the adjacent lamellae can be calculated for a crystal at a given tilt angle. This value then is corrected for the absorption of the X-rays before reaching the lamella and for the reflected X-rays from the lamella to the back of the crystal, thereby simulating the rocking curve.

The reflectivity and integrated reflectivity of bent Laue crystals also can be calculated analytically. The normalized thickness, A, of the lamella, in units of extinction length is

$$A = T_l/L_{\mathrm{ex}}, \tag{5}$$

where $L_{\mathrm{ex}} = V_c(\gamma_0\gamma_H)^{1/2}/(r_e\lambda KF_H)$ is the extinction length, V_c is the volume of the unit cell, $\gamma_H = \cos(\chi \pm \theta_B)$, r_e is the classical electron radius, λ is the X-ray wavelength, K is the polarization factor and F_H is the structure factor. For Laue crystals, if A is chosen as

$$A = R_s BQ, \tag{6}$$

then the integrated reflecting power, I, is approximately (Erola *et al.*, 1990)

$$I \cong (\tanh A/A)(Q/a\mu)\exp(-\mu T_0/\gamma_H)[1 - \exp(-a\mu T_0/\gamma_0)], \tag{7}$$

where $a = 1 - \gamma_0/\gamma_H$, T_0 is the thickness of the crystal, μ is the linear attenuation coefficient and Q is the integrated reflecting power per unit length at the kinematical limit (Zachariasen, 1945)

$$Q = r_e^2 K^2(F_H^2\lambda^3/\sin 2\theta_B). \tag{8}$$

Equation (7) gives about 10–20% accuracy.

For high-energy X-rays that are the primary focus for sagittally bent Laue crystals, the rocking curve is approximately rectangular, with a width of (Zhong *et al.*, 2002)

$$\omega \cong [\Delta\theta^2(T_0) + \omega_a^2]^{1/2}, \tag{9}$$

where ω_a is the Darwin width of the reflection used. The reflectivity then is calculated using (9) and (7):

$$R \cong I/\omega. \tag{10}$$

3. Experimental method

Perfect silicon crystals, widely used as X-ray monochromators, were bent sagittally to test the model. Rocking curves of low-
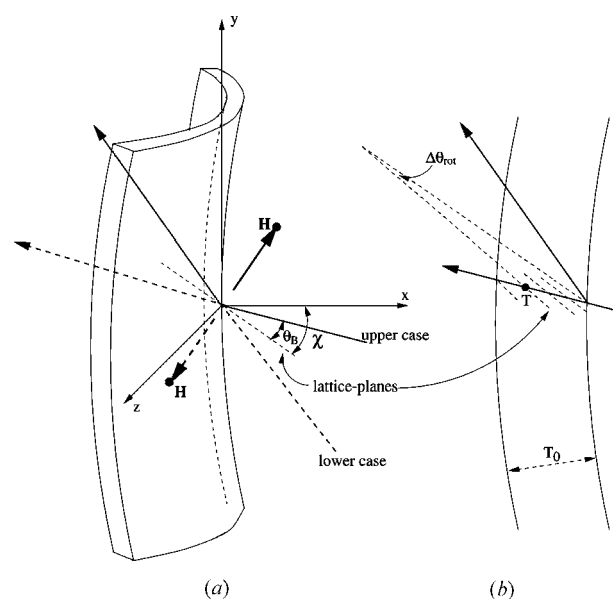

Figure 1
Lamellar model for a sagittally bent Laue crystal. (*a*) Coordinate system used, and (*b*) cross section in the diffraction plane, showing the change in the angle and the *d* spacing of the lamellae along the incident beam.

Table 1
Orientation of the four crystals used in the experiment and the parameters for the simulation.

x (surface normal)	[100]	[511]	[111]	[111]
y (bending axis)	[011]	[$\bar{2}$55]	[1$\bar{1}$0]	[$\bar{2}$11]
z (diffraction zone)	[0$\bar{1}$1]	[0$\bar{1}$1]	[112]	[0$\bar{1}$1]
S'_{13}	−0.36	−0.34	−0.16	−0.16
S'_{23}	−0.061	−0.083	−0.26	−0.26
S'_{63}	0	0.16	0	0.28
CS'_{23}, measured	−0.040	−0.058	−0.19	−0.19

index reflections with typical widths of tens to hundreds of microradians, and reflectivities of tens of percent, can be conveniently measured using a collimated monochromatic pencil beam. Fig. 2 is a scheme of the experimental set-up, at the X17B1 beamline of the National Synchrotron Light Source (NSLS).

The incident beam, of 67 keV energy, was generated by a silicon 220 Laue–Bragg monochromator, and defined by tungsten slits to a size 0.1 mm high by 0.5 mm wide. The monochromatic beam had an energy bandwidth of 10^{-4} ($\Delta E/E$) and a vertical divergence of about 10 μrad. The intensities of the incident and the diffracted beams were measured by identical ion chambers filled with argon gas at atmospheric pressure. The measured reflectivity was corrected for absorption by the argon gas in the first ion chamber and in the air path between the ion chambers. To avoid broadening the rocking curves due to the non-uniform bending of the crystal, the incident beam was limited horizontally to 0.5 mm wide. This width was expanded to 3 mm to verify that the rocking curves were not affected. The pencil beam was incident on the middle of the crystals.

Since the model predicts a strong dependence of the rocking curve on the crystal's orientation and the asymmetry angle of the reflection used, measurements were made on a variety of low-index reflections on four crystals of different orientations. The orientations of the crystals with respect to their sagittal bending are shown in Figs. 3(a), (b), (c) and (d). These include a (100) crystal (surface perpendicular to the [100] crystallographic direction) bent around the [011] direction, a (511) crystal bent around [$\bar{2}$55], and two (111) crystals, bent around [1$\bar{1}$0] and [$\bar{2}$11], respectively.

Each crystal was cut from a single-side polished silicon wafer, 0.67 mm thick with appropriate surface orientation, into a rectangle of 40 by 100 mm, so that its short edges were parallel to the sagittal bending axis. The center area, 40 mm high by 57 mm wide, was bent to the desired radius using a
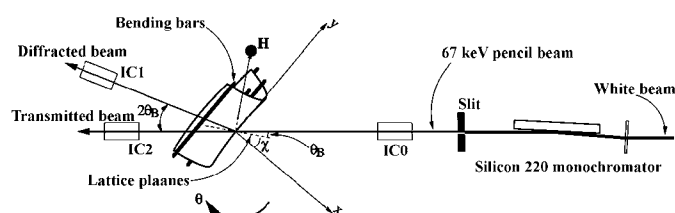
four-bar bender, a device with parallel bars that introduces approximately equal and opposite bending moments. The bending was set by focusing a laser beam with the polished side of the crystal. The sagittal and anticlastic bending radii then were determined by shift in the centroid of rocking curves measured at different locations on the crystal.

The sagittal bending radii used ranged between 0.5 and 3 m. For each crystal bent to a specific radius, rocking curves were measured on different reflections belonging to the same zone whose axis coincides with the z axis, as shown in Fig. 3.

4. Experimental results and analysis

The rocking curve's width, reflectivity and integrated reflectivity were simulated for all the reflections measured, using (3), (7) and (10). The upper sign was used for all reflections measured (Fig. 3). We used the measured Poisson ratio to calculate the CS'_{32} for each crystal. The other elastic compliances were calculated by a transformation of the stress–strain tensor of the principal compliances for silicon (Wortman & Evans, 1965). Table 1 lists the parameters used for the simulation of the four crystals.

To illustrate the general characteristics of the rocking curves measured, Fig. 4 shows the rocking curves of the $\bar{1}$11 ($\chi = -35.3°$), $\bar{1}$33 ($\chi = -13.3°$), $\bar{3}$33 ($\chi = -35.3°$), $\bar{3}$11 ($\chi = -64.8°$) and 022 ($\chi = 0$) reflections on the (100) crystal, sagittally bent to a radius of 0.76 m. Since all the reflections are in the second quadrant of Fig. 3(a), they have negative or zero asymmetry angles. The rocking curves of their symmetry-related reflections in the first quadrant, with positive asymmetry angles, are similar. The curves which are wider than 30 μrad are roughly rectangular, typical of bent Laue crystals
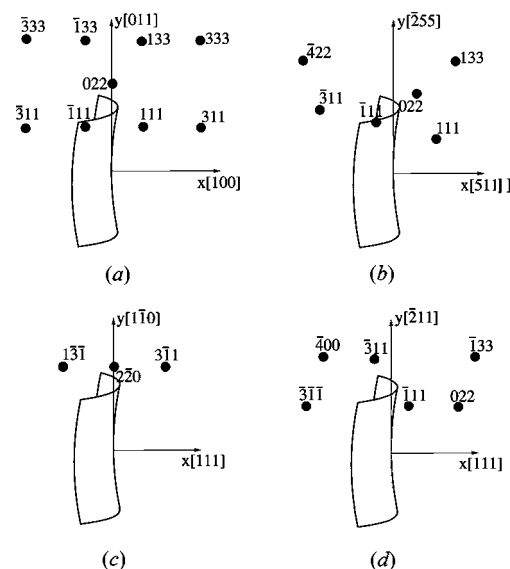

Figure 2
Experimental set-up for the rocking-curve measurements.

Figure 3
Real- and reciprocal-space configurations of the four crystals used for the experiment. (a) A (100) crystal, sagittally bent around the [011] direction, and diffracting in the 0$\bar{1}$1 zone; (b) a (511) crystal bent around the [$\bar{2}$55] direction, and diffracting in the 0$\bar{1}$1 zone; (c) a (111) crystal bent around the [1$\bar{1}$0] direction, and diffracting in the 11$\bar{2}$ zone; and (d) a (111) crystal bent around the [$\bar{2}$11] direction and diffracting in the 0$\bar{1}$1 zone.

Table 2
Comparisons between the measured and simulated rocking-curve width, reflectivity (R), and integrated reflectivity (I) of the {311} and {111} reflections on four different crystals; the normalized lamellar thickness, A, is also given.

Normal	(100)			($5\bar{1}1$)			(111)	($\bar{1}11$)		
Bending axis	[011]			[$\bar{2}55$]			[$1\bar{1}0$]	[$\bar{2}11$]		
R_s (m)	0.76			0.95			0.80	0.80		
Reflection	$\bar{1}11$	$\bar{3}11$	111	$\bar{3}11$	$\bar{1}11$	111	$3\bar{1}1$	$\bar{3}\bar{1}1$	$\bar{3}11$	$\bar{1}11$
χ (°)	−35.3	−64.8	35.3	−49.0	−19.5	51.0	31.5	−60.5	−10.0	19.5
A	0.82	1.4	0.89	0.32	0.53	20	0.28	0.17	0.12	0.30
ω, model (μrad)	111	37	107	110	150	7.5	106	264	200	273
FWHM (μrad)	122	31	118	105	145	17	132	233	203	272
R, model	0.64	0.79	0.68	0.29	0.46	0.79	0.26	0.16	0.12	0.28
R, meas.	0.59	0.76	0.56	0.28	0.43	0.15	0.17	0.17	0.11	0.28
I, model (μrad)	71	30	72	32	70	5.9	28	41	23	76
I, meas. (μrad)	72	24	68	29	63	3.0	22	40	22	77

diffracting at high X-ray energies. The rocking curve for the 022 reflection ($\chi = 0$) is extremely narrow, as predicted by (3), which gives the Darwin width (3 μrad) of the reflection. Owing to the divergence and energy resolution of the incident beam, the measured rocking curve is approximately triangular with a reflectivity less than theoretical prediction. Nevertheless, the integrated reflectivity of this reflection agrees with the theory.

Fig. 4 shows that the width of the rocking curve changes depending on the asymmetry angle of the reflection used. As χ changes from 0 (022 reflection) to −65° ($\bar{3}11$), the rocking-curve's width increases from 10 to 120 μrad for the $\bar{1}11$ reflection, then decreases to about 30 μrad for the $\bar{3}11$ reflection. The rocking-curve width is directly related to $\Delta\theta(T_0)$, calculated using (3). Ignoring $\Delta\theta_B(T)$ due to small Bragg angle at 67 keV, and considering that $S'_{63} = 0$ and CS'_{23} (−0.04) is small for this crystal, the term $S'_{13} \sin\chi \cos\chi$ dominates. Thus, at $\chi = 0$, $\Delta\theta(T_0) = 0$; at $\chi = -35.3°$, $\Delta\theta(T_0)$ reaches near a maximum, and decreases with χ approaching 65° ($\bar{3}11$ reflection). This phenomenon is different in meridionally bent crystals whose integrated reflectivity typically increases with asymmetry angle.

The harmonic reflections, $\bar{1}11$ and $\bar{3}33$, which have the same asymmetry angle, have similar rocking-curve widths (Fig. 4). The kinematic limits of integrated reflectivity are 86 and 11 μrad for the $\bar{1}11$ and $\bar{3}33$ reflections, respectively, a factor of
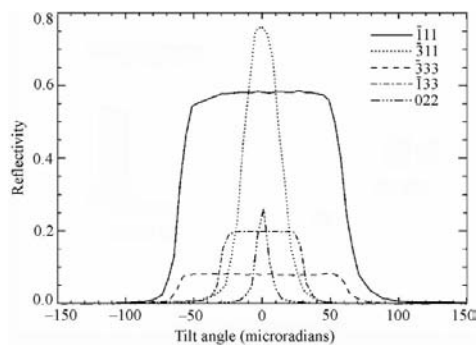
8 difference. The normalized lamellar thicknesses, A, are 0.82 and 0.093 for the $\bar{1}11$ and $\bar{3}33$ reflections, respectively, indicating that the latter approached the kinematic limit at the sagittal-bending radius (0.76 m) used, while the $\bar{1}11$ diffraction was more dynamical, owing to its large structure factor. This explains why their measured reflectivities differ only by about a factor of 5.

The measured and simulated parameters for the rocking curves of the $\bar{1}11$ and $\bar{3}11$ reflections are summarized in Table 2, which shows the agreement between the theoretical and experimental values of the rocking-curve widths and reflectivities.

Fig. 5 shows examples of the rocking curves of the [$0\bar{1}1$]-zone reflections on the (111) crystal bent according to Fig. 3(d). Unlike the (100) crystal discussed above, this crystal lacks mirror symmetry across the plane perpendicular to the bending axis, and has a large S'_{63} (0.28). $S'_{63} \cos^2\chi$ contributes to the rocking-curve width if χ is positive, but cancels the contributions of other terms if χ is negative. Thus, there is a large difference between the first-quadrant reflections ($\bar{1}11$, $\bar{1}33$ and 022) and the corresponding second-quadrant ones ($\bar{3}11$, $\bar{4}00$ and $\bar{3}\bar{1}1$).

In particular, the $\bar{4}00$ ($\chi = -35.3°$) and $\bar{1}33$ ($\chi = 41.5°$) reflections have similar but opposite asymmetry angles and similar structure factors, yet their rocking curves are drastically different, with $\bar{4}00$ having a width of 50 μrad and diffracting close to the dynamical limit ($A = 1.1$), and $\bar{1}33$
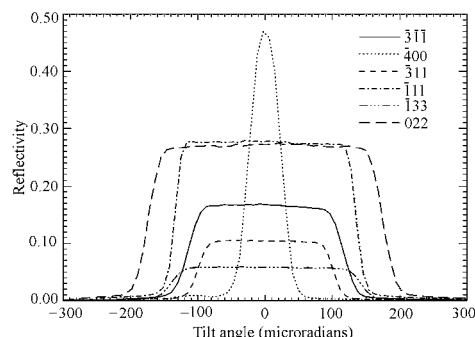

Figure 4
Measured rocking curves of the [$0\bar{1}1$] zone reflections on a (100) crystal, sagittally bent to a radius of 0.76 m. Only the reflections with $\chi \leq 0$ are shown. Other symmetry-related reflections in the same zone have similar rocking curves.

Figure 5
Measured rocking curves of the [$0\bar{1}1$]-zone reflections on a (111) crystal, sagittally bent around [$\bar{2}11$] to a radius of 0.80 m.

having a width of 284 µrad and diffracting close to the kinematic limit ($A = 0.073$). The measured rocking-curve widths varied between 50 and 350 µrad, demonstrating a wide range of diffraction properties achievable on this crystal by varying the magnitude and sign of the asymmetry angles of the reflections.

Fig. 6 shows the rocking curves of the $[0\bar{1}1]$-zone reflections on the (511) crystal, sagittally bent according to Fig. 3(b). There are two {111} reflections with different asymmetry angles ($\chi = 51.1°$ and $-19.5°$ for 111 and $\bar{1}11$ reflections, respectively). The rocking curves of the two reflections are dramatically different. Equation (3) shows that, for the 111 reflection, the effects of S'_{63} (0.16) cancel the contributions of other factors, leading to a near-zero rocking-curve width and, as a result, small integrated reflectivity close to the dynamical limit. Table 2 shows that the measured reflectivity is less than the expected near-unity, and the measured width is larger than the theoretical one. As with the 022 reflection on the (100) crystal, this difference can be explained by the divergence of the incident beam and the mismatch between the monochromator's reflection (220) and the reflection measured (111).

Owing to their large reflecting power, the low-index reflections, 111 and 113, free of second harmonics, are particularly useful for monochromators and analyzers. Table 2 shows detailed comparisons of our experimental and simulation results for these reflections for the four crystals tested. They show that the model correctly accounts for a wide range of rocking-curve properties achieved by the same reflection on different crystals, or on the same crystal with different asymmetry angles.

For the (100) crystal sagittally bent around $[\bar{2}11]$, the rocking curves of the $[0\bar{1}1]$-zone reflections were measured at different sagittal-bending radii. Fig. 7(a) shows the dependence of the measured width (FWHM) of the rocking curves on the sagittal bending curvature, $1/R_s$, and the theoretical relationship, calculated using (3) and (9). Experimental widths are slightly larger than the theoretical ones, owing mostly to the mismatch between the dispersion of the reflections of the monochromator and the bent crystal, and the vertical divergence of the incident beam. In the range of curvature tested,
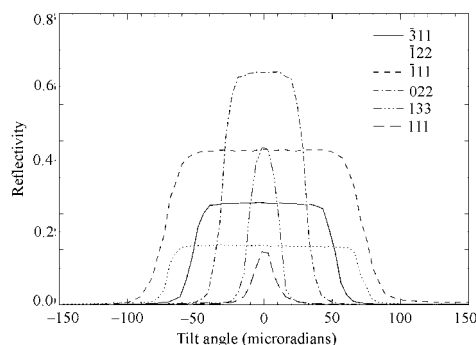
there is a linear relationship between the rocking-curve width and the curvature. The rocking-curve widths differ for different reflections, in agreement with the theory.

Fig. 7(b) shows the reflectivity of these reflections *versus* the sagittal bending curvature, and the theoretical relationship calculated using (10). For a given reflection, the reflectivity generally is close to unity for a small curvature (weak bending corresponding to the dynamical diffraction limit) and decreases with increasing curvature. The curvature at which this change takes place depends on the reflection, a trend in agreement with the theory.

The integrated reflectivity, I, is defined as the area under the rocking curves. Fig. 7(c) shows the measured and theoretical integrated reflectivity of the rocking curves, and the kinematic limit for each reflection. The integrated reflectivity increases with the curvature to approach the kinematical limit.

Figs. 7(a), (b) and (c) show good agreement between theory and experiment, especially for the integrated reflectivity, that is not affected by the divergence and energy distribution of the incident beam. The model correctly predicts the effects of the change in sagittal bending radii on the rocking curve of each reflection, suggesting its applicability for a wide range of bending radii and reflections in the region between the kinematic and dynamical limits.
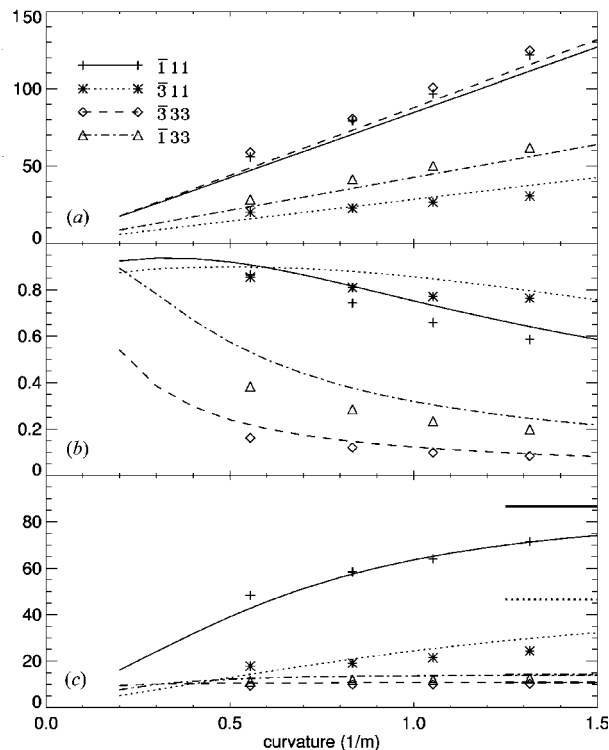

Figure 6
Rocking curves measured of the $[0\bar{1}1]$ zone reflection on a (511) crystal, sagittally bent around $[\bar{2}55]$ to a radius of 0.95 m.

Figure 7
(a) Width (µrad), (b) reflectivity, and (c) the integrated reflectivity (µrad) of the rocking curves at different sagittal bending curvatures. The rocking curves were measured using the $[0\bar{1}1]$-zone reflections on the (100) crystal sagittally bent around $[\bar{2}11]$. The lines show the theoretical relationships. The horizontal lines in (c) show the kinematic limits for the integrated reflectivity of the reflections.

research papers

5. Discussion

We developed a lamellar model to calculate the rocking curves of sagittally bent Laue crystals. The model was verified experimentally by rocking-curve measurements, using various reflections on four silicon crystals of different orientations. The reflectivity and width of the rocking curves corresponded with those predicted by the model.

Our experimental results illustrate that a variety of diffraction properties are attainable by sagittally bent Laue crystals. The model allows insight into the key factors affecting X-ray diffraction by these crystals, including the crystal's orientation, anisotropy and bending radius. This knowledge allows the design of the monochromator to be optimized to fit different experimental needs, which include consideration on flux (related to the reflectivity and integrated reflectivity of the crystal) and resolution (related to the anticlastic bending radius and the rocking-curve width).

The sagittal focal length is $R_s/(2 \sin \theta_B \sin \chi)$. For high-energy X-rays, strong sagittal bending of the order of 1 m radius and a low-index reflection with a large asymmetry angle is needed to achieve the focal length of about 10 m required for typical synchrotron X-ray beamlines. For experiments also requiring good energy resolution, we showed, by both experiments and simulation, that a few reflections on high-symmetry crystals are good candidates; these include the $3\bar{1}1$ reflection on a (100) crystal bent around [011], and the 400 reflection on a (111) crystal bent around [$\bar{2}$11]. Also, the 111 reflection on a (511) crystal provides an energy resolution similar to that of a perfect crystal.

References

Albertini, G., Boeuf, A., Cesini, G., Mazkedian, S., Melone, S. & Rustichelli, F. (1976). *Acta Cryst.* A**32**, 863–868.
Batterman, B. W. & Cole, H. (1964). *Rev. Mod. Phys.* **36**, 681–717.
Boeuf, A., Lagomarsino, S., Mazkedian, S., Melone, S., Puliti, P. & Rustichelli, F. (1978). *J. Appl. Cryst.* **11**, 442–449.
Egert, V. G. & Dachs, H. (1970). *J. Appl. Cryst.* **3**, 214–220.
Erola, E., Eteläniemi, V., Suortti, P., Pattison, P. & Thomlinson, W. (1990). *J. Appl. Cryst.* **23**, 35–42.
Kalman, Z. H. & Weissmann, Z. (1983). *J. Appl. Cryst.* **16**, 295–303.
Krisch, M., Freund, A., Marot, G. & Zhang, L. (1991). *Nucl. Instrum. Methods Phys. Res. A*, **305**, 208–213.
Mikula, P., Kulda, J., Vrana, M. & Chalupa, B. (1984). *J. Appl. Cryst.* **17**, 189–195.
Penning, P. & Polder, D. (1961). *Philips Res. Rep.* **16**, 419–440.
Schulze, C. & Chapman, D. (1995). *Rev. Sci. Instrum.* **66**, 2220–2223.
Suortti, P. & Schulze, C. (1995). *J. Synchrotron Rad.* **2**, 6–12.
Suortti, P. & Thomlinson, W. (1988). *Nucl. Instrum. Methods*, A**269**, 639.
Suortti, P., Thomlinson, W., Chapman, D., Gmür, N., Greene, R. & Lazarz, N. (1990). *Nucl. Instrum. Methods*, A**297**, 268–274.
White, J. E. (1950) *J. Appl. Phys.* **21**, 855–859.
Wortman, J. J. & Evans, R. A. (1965). *J. Appl. Phys.* **36**, 153–156.
Yoneda, Y., Matsumoto, N., Furukawa, Y. & Ishikawa, T. (2001). *J. Synchrotron Rad.* **8**, 18–21.
Zachariasen, W. H. (1945). *Theory of X-ray Diffraction in Crystals*, Section III.7, pp. 106–108. New York: Wiley.
Zhong, Z., Kao, C. C., Siddons, D. P. & Hastings, J. B. (2001a). *J. Appl. Cryst.* **34**, 504–509.
Zhong, Z., Kao, C. C., Siddons, D. P. & Hastings, J. B. (2001b). *J. Appl. Cryst.* **34**, 646–653.
Zhong, Z., Kao, C. C., Siddons, D. P. & Hastings, J. B. (2002). *Acta Cryst.* A**58**, 487–493.